Supporting Information for "Inverse Design and Synthesis of Acac-Coumarin Anchors for Robust TiO_2 Sensitization"

Dequan Xiao, Lauren A. Martini, Robert C. Snoeberger III,
Robert H. Crabtree*, and Victor S. Batista*

Department of Chemistry, Yale University, New Haven, CT 06520

* Corresponding Email address: Victor.Basita@yale.edu; Robert.Crabtree@yale.edu

1. TB-LCAP optimization results.

The TB-LCAP search results for maximum $f_{HL}P(\lambda_{HL})$ are performed as described in Sec. 2. All optimized structures are available upon request.

2. Density of states analysis.

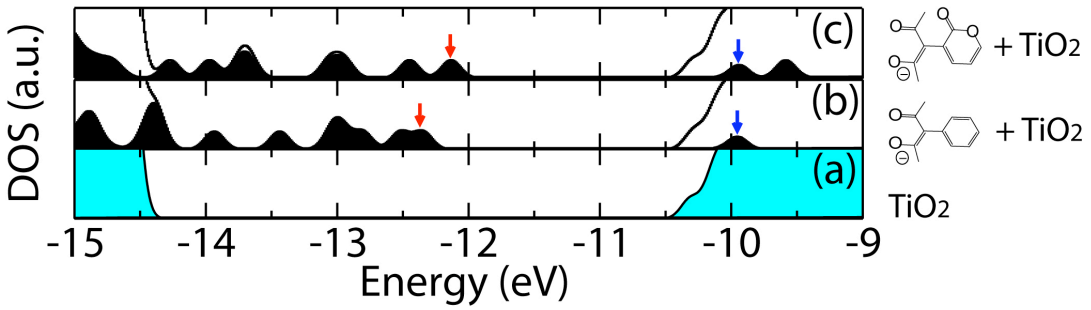

Figure S1. Density of states (DOS) for the periodic structures of TiO_2 anatase (a), phenyl-acac-TiO_2 (b), and 3-acac-pyran-2-one-TiO_2 (c), calculated at the extended Hückel level. The filled black lines in (b)-(c) are the projected DOS of the dye chromophores. The blue arrows point to the electronic states with a predominant contribution of HOMO, and the red arrows point to the electronic states with a predominant contribution of LUMO. Here, the DOS of (a)-(c) sampled at γ-point of the periodic systems are consistent with that of (a)-(c) in Figure 9 (of the paper) calculated based on the finite-sized nanostructures.

3. Extending the π-conjugation of 3-acac-pyran-2-one using 3 $-CH_2=CH_2-$ units.

Note that, due to the size limit of 4-acac-coumarin, the calculated oscillator strength for 4-coumarin-acac adsorbed on $[Ti_2O_2(OH)_2(H_2O)_4]^{2+}$ is about 0.02, while the C343 dye molecule adsorbed on $[Ti_2O_2(OH)_2(H_2O)_4]^{2+}$ shows visible oscillator strengths at the scale of 0.8 (see section 4 of SI). To achieve large visible oscillator strength (or intense absorption) in practice, we suggested synthesizing 3-acac-pyran-2-one derivatives (or coumarin-acac derivatives) with expanded π-conjugation or

added donor/acceptor groups. For example, by expanding the π-conjugation of 3-acac-pyran-2-one with 3 $–CH_2=CH_2-$ units (see the structure in Figure S2a), we can obtain the visible oscillator strength of 0.80 (Figure S2b-c), making it a comparable dye to C343. This large oscillator strength is generated by the HOMO to LUMO+4 transition (Figure S2c) where both molecular orbitals are delocalized on the π-conjugate including the alkene groups and pyran-2-one ring. As a comparison (see section 5 in SI), extending phenyl-acac using 3 $–CH_2=CH_2-$ units shows much weaker absorption bands in the visible light region. Hence, we suggest using 3-acac-pyran-2-one as a lead chromophore.

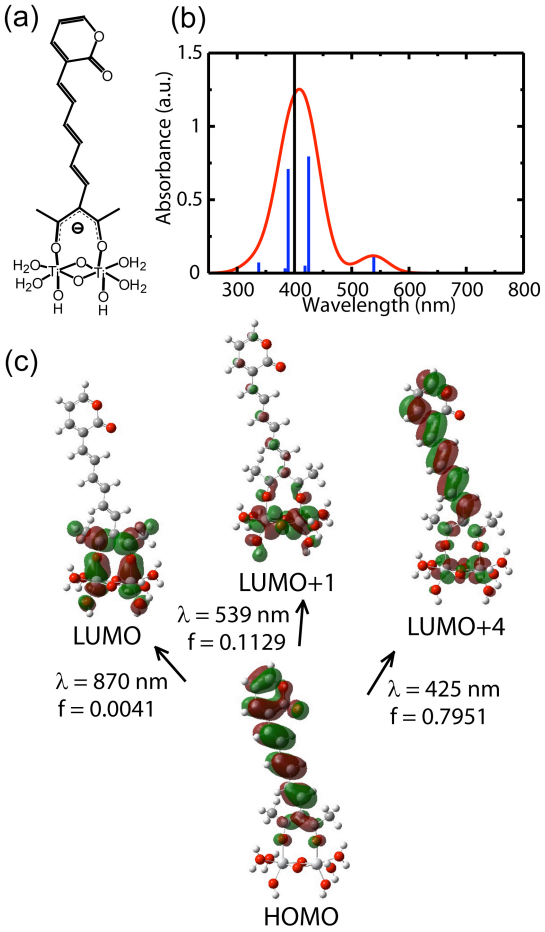

Figure S2. Structure of 3-acac-pyran-2-one adsorbed a $[Ti_2O_2(OH)_2(H_2O)_4]^{2+}$ model (a), photo-absorption spectrum calculated by TD-DFT (b), and characteristic electronic transitions (c). In (a), a Gaussian function with fwhm = 60 *nm* is used to broaden of the oscillator strengths to facilitate the visualization of photo-absorption spectrum. Here, λ denotes the transition wavelength, and f denotes the oscillator strength.

Electron injection for the extended 3-acac-pyran-2-one with 3 $–CH_2=CH_2-$ units. As shown in Figure S3, the electron can be injected from the LUMO+4 (DFT) or LUMO (DFT) of the expanded 3-acac-pyran-2-one with 3 $–CH_2=CH_2-$ units to the TiO_2 surface.

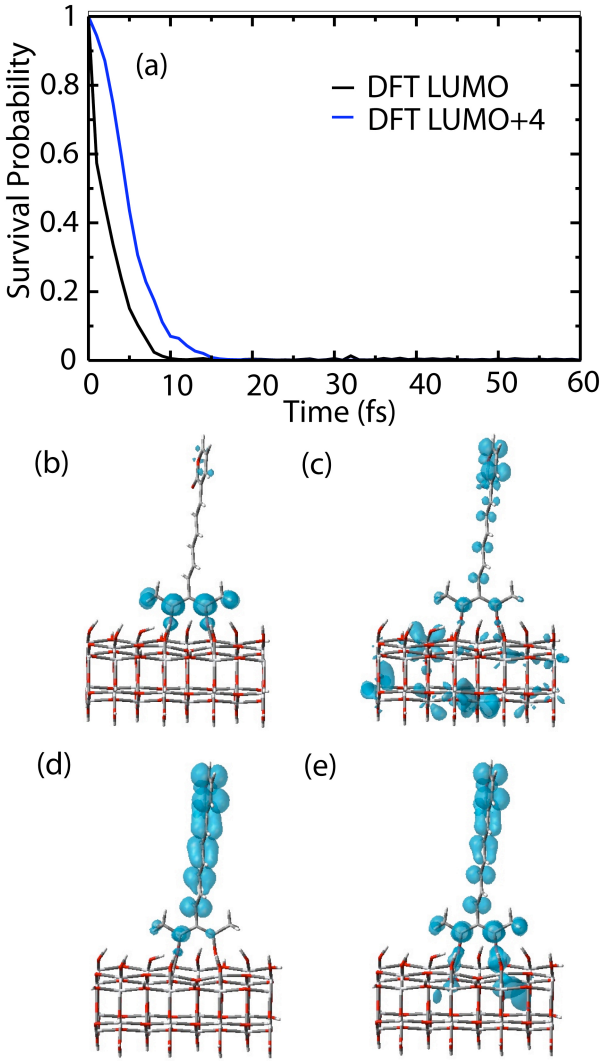

Figure S3. Interfacial electron injection from the LUMO (DFT) and LUMO+4 (DFT) of the expanded 3-acac-pyran-2-one with 3 $–CH_2=CH_2-$ units to the TiO_2 anatase supercell, simulated by the quantum dynamics in the extended Hückel theory. The electron survival probabilities on the 4-acac-coumrain LUMO and LUMO+4 decay at a time of 10 *fs* and 15 *fs* respectively (a), and the snapshots are shown for the electronic charge distribution, at t = 0 *fs* for the LUMO (b) and at t = 6 *fs* for the LUMO (c), at t = 0 *fs* for the LUMO+4 (d), and at t = 6 *fs* for the LUMO+4 (e).

4. TD-DFT absorption spectrum for C343 coumarin dye adsorbed on TiO_2

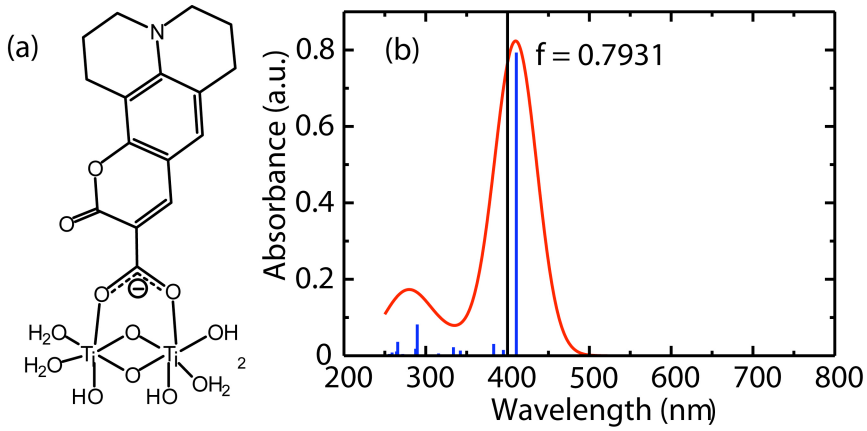

Figure S4. Structure of C343 coumarin dye adsorbed a $[Ti_2O_2(OH)_2(H_2O)_4]^{2+}$ model (a), photo-absorption spectrum calculated by TD-DFT (b), where a Gaussian function with fwhm = 60 nm is used to broaden of the oscillator strengths to facilitate the visualization of photo-absorption spectrum. Here, f denotes the oscillator strength.

5. TD-DFT absorption spectrum for extended phenyl-acac adsorbed on TiO_2

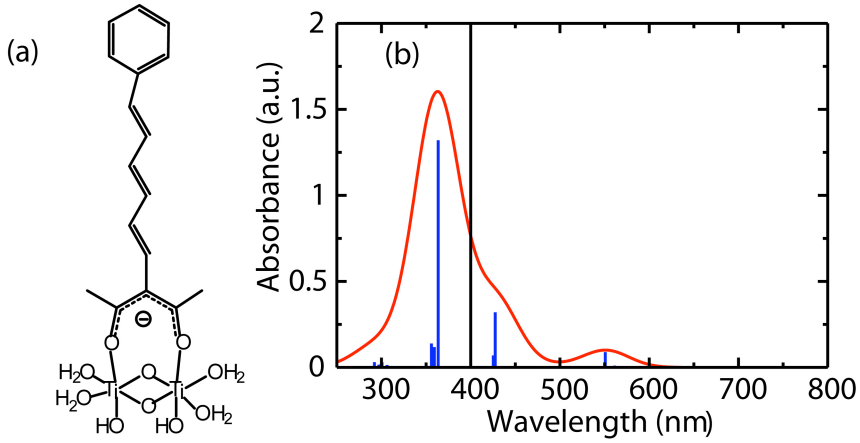

Figure S5. Structure of the extended phenyl-acac with 3 $–CH_2=CH_2-$ units adsorbed a $[Ti_2O_2(OH)_2(H_2O)_4]^{2+}$ model (a), photo-absorption spectrum calculated by TD-DFT (b), where a Gaussian function with fwhm = 60 nm is used to broaden of the oscillator strengths to facilitate the visualization of photo-absorption spectrum.

6. Comparison of absorption spectra calculations between the TD-DFT and the extended Hückel methods

Without specifically optimizing the extended Hückel parameters for photo-absorption spectrum calculations, we show here that the extended Hückel photo-absorption calculation is consistent with the TD-DFT photo-absorption calculations, especially in terms of the nature of the electronic transitions, making it plausible to be used in the TB-LCAP optimization algorithm. Here, we compute the extended Hückel photo-absorption spectrum for 4-acac-coumarin using the same optimized geometry for the TD-DFT calculation. Figure S6a shows the extended Hückel photo-absorption spectra of 4-acac-coumarin, together with the characteristic electronic transitions

shown in Figure S6c. Compared to the TD-DFT photo-absorption spectrum (Figure 9a in the paper), the extended Hückel spectrum red-shifts for about 100 *nm*. However, the electronic nature of the HOMO-LUMO transition (that generates the strongest visible oscillator strength) is consistent with that by the TD-DFT calculation. For 3-acac-coumarine adsorbed on a TiO_2 slab, the extended Hückel photo-absorption spectrum is shown in Figure S6b, with the characteristic electronic transitions shown in Figure S6d. Compared to the TD-DFT spectrum (Figure 10a in the paper), the extended Hückel spectrum red-shifts for about 60 *nm*. The electronic nature of the HOMO-LUMO transition calculated by extended Hückel using the TiO_2 slab is consistent with that calculated by the TD-DFT method using the $[Ti_2O_2(OH)_2(H_2O)_4]^{2+}$ model. By comparing Figure S6 a and b, the spectrum is blue-shifted as 4-acac-coumarin is attached to TiO_2. This trend is consistent with the blue-shift shown by the TD-DFT calculation by comparing Figures 11a and 12a in the paper.

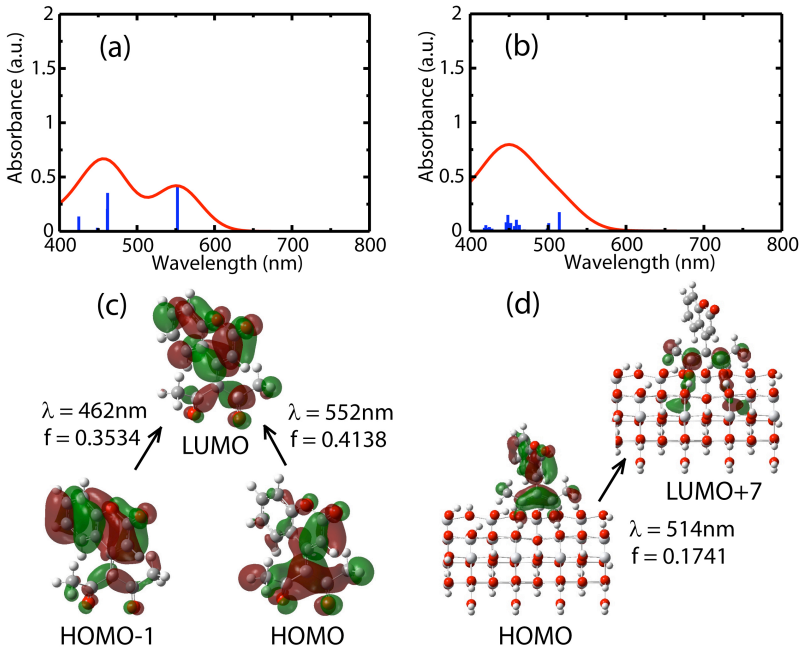

Figure S6. Extended Hückel photo-absorption spectra for 4-acac-coumarin in gas phase (a) and adsorbed on a TiO_2 slab (b). The characteristic electronic transitions of (a) is shown in (c), and the characteristic electronic transitions of (b) in shown in (d). In (a) and (b), a Gaussian function with fwhm = 60 *nm* is used to broaden of the oscillator strengths to facilitate the visualization of photo-absorption spectrum. Here, λ denotes the transition wavelength, and *f* denotes the oscillator strength.

7. Absorption spectrum of phenyl-acac

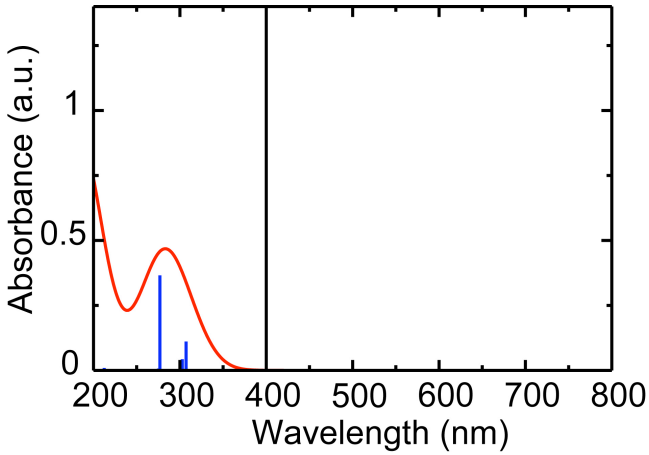

Figure S7. Photo-absorption spectrum for phenyl-acac anion in methanol solution calculated by TD-DFT with the polarizable continuum solvent model.

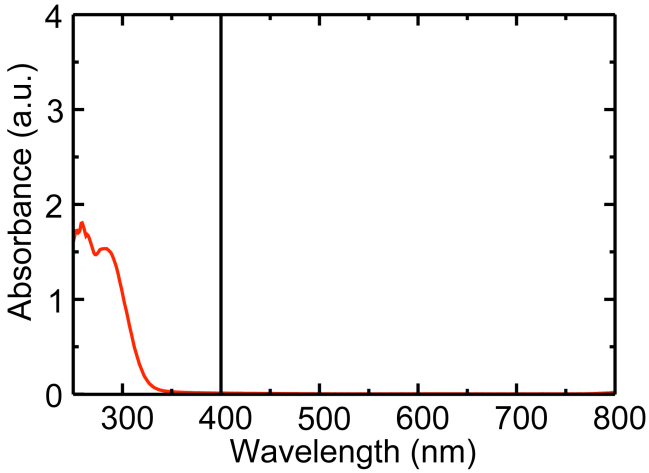

Figure S8. Photo-absorption spectrum measured experimentally for phenyl-acac anion (formed by deprotonation of **1** using one equivalent of tetrabutylammonium hydroxide) in 2.0×10^{-3} M methanol solution.

8. Surface contour of TB-LCAP

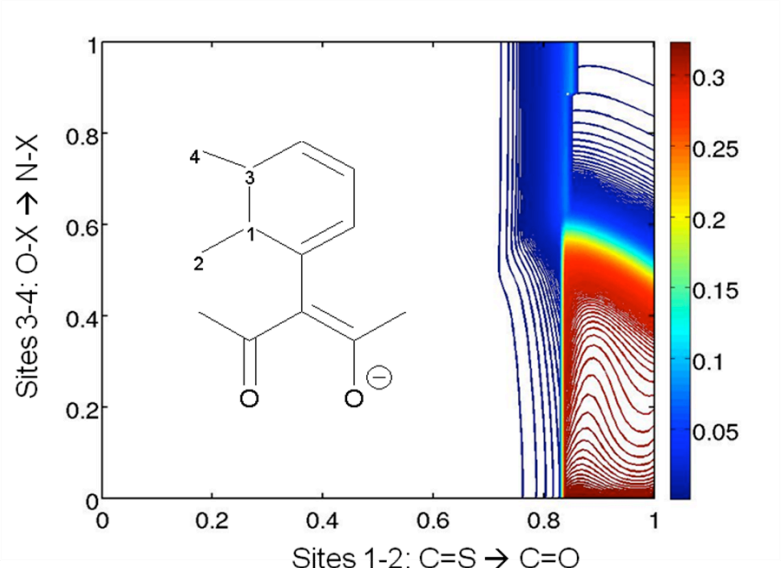

Figure S9. Surface contour of $f_{HL}P(\lambda_{HL})$ that is formed by varying C=S to C=O at sites 1 and 2, and by varying O-X to N-X at sites 3 and 4.